Journal of Power Sources 195 (2010) 5666–5673

Contents lists available at ScienceDirect

Journal of Power Sources

journal homepage: www.elsevier.com/locate/jpowsour

Electrical stability of a novel sealing glass with (Mn,Co)-spinel coated Crofer22APU in a simulated SOFC dual environment

Y.-S. Chou*, J.W. Stevenson, G.-G. Xia, Z.-G. Yang

K2-44, Energy and Efficiency Division, Pacific Northwest National Laboratory, P.O. Box 999, Richland, WA 99354, United States of America

ARTICLE INFO

Article history:
Received 16 December 2009
Received in revised form 12 March 2010
Accepted 15 March 2010
Available online 19 March 2010

Keywords:
Electrical stability
Sealing glass
Interface
Crofer22APU
SOFC

ABSTRACT

A novel alkaline-earth silicate (Sr–Ca–Y–B–Si–Zn) sealing glass was developed for solid oxide fuel cell (SOFC) applications. The glass was sandwiched between two metallic interconnect plates and tested for electrical stability in a dual environment at elevated temperatures of 800–850 °C. A ferritic stainless steel (Crofer22APU) was used as the metallic interconnect material in the as-received state and coated with $(Mn,Co)_3O_4$ spinel. The isothermal aging results showed stable electrical resistivity at 800–850 °C for ~500–1000 h. The electrical resistivities at 800 or 850 °C of the spinel coated samples were lower than the as-received ones; however, they were still several orders of magnitude higher than typical SOFC functional parts. Interfacial microstructure was characterized and possible reactions are discussed.

1. Introduction

One of the major hurdles for advancing solid oxide fuel cell (SOFC) technologies is a robust and durable sealing material or system. The challenges lie in all aspects of material properties: thermal, mechanical, chemical and electrical, and include not only bulk properties but also interfaces such as metallic interconnect to glass or electrolyte to glass [1–5]. The sealing materials have to provide hermeticity or low leak rate, and must be electrically insulating, chemically compatible with mating materials, thermally stable and durable in the harsh dual operating environment (oxidizing vs. wet reducing atmospheres). In addition, the seals must survive thermal cycling and exhibit long-term stability (e.g., ~40,000 h) and in some cases vibrational stability while operating at elevated temperatures (~700–850 °C).

Recent studies of sealing glasses for SOFC applications have been focused primarily on alkaline-earth based silicates such as Ba–Ca–Al–B–Si glass with a target operating temperature of ~750 °C [6] and Sr–Ca–Y–B–Si with a focus on achieving higher sealing temperatures (>950 °C) by varying the B_2O_3 content [7]. The refractory type of sealing glass showed very stable microstructure, crystalline phases and thermal expansion coefficient (CTE) even after 2000 h aging at 900 °C [7]. Lahl et al. studied the influence of nucleating agents (e.g., TiO_2 and ZrO_2) on the activation energy of crystal growth of various glasses A–Al–Si–B glasses (A = Ba, Ca, Mg) [8]. Sohn et al. investigated the thermal and chemical stability of the Ba–La–Al–B–Si system. They found that the CTE of the bulk glass increased with BaO content and a maximum CTE of $\sim 11 \times 10^{-6}/°C$ was obtained at BaO = 40% and B_2O_3/SiO_2 = 0.7% [9]. Ley et al. studied the glass system of Sr–Al–La–B–Si and concluded that the CTE of the bulk glasses could be tailored in the range of $8–13 \times 10^{-6}/°C$ [10].

In recent years, SOFC materials' development has focused on anode-supported thin electrolyte cells such that the operation temperatures can be lowered from ~1000 to ~800 °C or lower, which makes the use of metallic interconnect materials feasible. Therefore, recent research has focused on chemical compatibility as well as mechanical integrity of seal/interconnect structures. The behavior of various sealing glasses with Cr-containing ferritic stainless steels under SOFC environments was investigated [11–13], and the results for as-sealed or short-term aged (<400 h) samples all showed undesirable alkaline-earth chromate formation [7,13]. The formation of chromate along the glass/metal interfaces often degraded the strength substantially [14]; however, the strength reduction was minimized by aluminizing the metal surface [15]. In addition to the issues of Cr reaction with sealing glass at sealing areas, the Cr-poisoning effect on electrochemical performance of the cell was well recognized [16–18]. To minimize Cr migration at the cathode side, the metallic interconnect was often coated with a protective and electrically conducting oxide such as $(Mn,Co)_3O_4$ spinel [19–21]. Thus, it appears that one needs to have two coatings to use the Cr-containing ferritic stainless steels for SOFC applications: one for the sealing area and the other for the cathode air flow field. This presents a potential processing and cost challenge

* Corresponding author. Tel.: +1 509 3752527; fax: +1 509 3752186.
E-mail address: yeong-shyung.chou@pnl.gov (Y.-S. Chou).

0378-7753/$ – see front matter © 2010 Elsevier B.V. All rights reserved.
doi:10.1016/j.jpowsour.2010.03.052

Table 1
Chemical composition of sealing glasses.

Mole%	$SrCO_3$	CaO	Y_2O_3	B_2O_3	SiO_2	ZnO
YSO46	43.5	5.0	5.0	10.0	34.0	2.5

for SOFC technology, since the environments and temperatures for heat-treatment may be different for aluminization and spinel coatings. In this paper, we studied the electrical stability of a novel sealing glass with the $(Mn,Co)_3O_4$ spinel coated Crofer22APU in addition to thermal, chemical and mechanical behaviors. In general, the electrical resistivity of sealing glass was considered insulating comparing to values of SOFC cells and interconnects. However, recent study by Haanappel et al. on alkaline-earth silicate sealing glass with ferritic stainless steels showed excessive internal Cr oxidation for glass containing small amount of PbO, which led to the formation of highly conductive Fe-oxide dendrites for electrical shorting [22]. In this study, we have investigated the effect of coating, environment and temperature on the electrical stability of a novel alkaline-earth silicate sealing glass. Interfacial reaction and characterization were conducted on the as-received metal coupons and coated ones. The implication of $(Mn,Co)_3O_4$ spinel coatings on sealing area will be discussed in regard to SOFC applications.

2. Experimental

2.1. Glass making and test coupon preparation

The glass (designated YSO46) studied in this paper was a derivative of earlier developed "refractory" sealing glasses with a small addition of ZnO [7]. The chemical composition is listed in Table 1. The glass was prepared by melting constituent oxides and carbonates at ~1450 °C in a Pt crucible for half an hour in air. The details of the sealing glass fabrication and glass powder processing are given in Refs. [7,14]. Thermal properties of the as-cast glass and glass powder compacts sintered at elevated temperatures were measured with the dilatometer (Unitherm 1161, ANTER Corp., Pittsburgh, PA). The sintering temperature for glass powder compact was first heated to 550 °C and held for 2 h for binder burn-off, then to 950 °C and held for 2 h followed by 800 °C/4 h for crystallization in air. For sealing application, the glass powders were mixed with an organic binder (V-006, Heraeus Electronic Materials, W. Conshohocken, PA) to form a paste. A ferritic stainless steel, Crofer22APU (ThyssenKrupp, Germany), was selected for electrical stability tests. Crofer22APU is a leading candidate for metallic interconnect material due to good oxidation resistance, matching CTE with Ni/YSZ anode-supported YSZ cells, and the formation of conductive Cr-containing scales. The metal has a nominal composition of Cr (20–24% in wt.%), Mn (0.3–0.8%), Cu (0–0.5%), Al (0–0.5%), Si (0–0.5%) and traces of P, S and Ti [14]. The metal coupons were of square shape, one was 50 mm × 50 mm with a central square hole of 12 mm × 12 mm, the other was 25 mm × 25 mm. The metals were tested in the as-received state as well as after being coated with $(Mn, Co)_3O_4$ spinel. The processing for the spinel coating, which involved heat-treatment in a reducing environment followed by oxidation in air at elevated temperatures, is given in Ref. [19]. Electrical stability test samples were prepared by applying the glass paste between the two metal coupons to form steel/glass/steel sandwiches. After drying, the specimens were slowly heated to 550 °C for 2 h to remove organic binders. They were then fired to 950 °C/2 h followed by crystallization at 800 °C for 4 h in air. After cooling to room temperature, the joined metal couples were tested for leakage by applying a small amount iso-propanol in the central cavity to observe any penetration of the alcohol to the other side. For the electrical stability tests, only hermetic samples were used.

2.2. Electrical stability testing and microstructural characterization

The electrical stability tests were conducted in a simulated SOFC environment in which the glass seal was exposed to ambient air at one side and a humid reducing environment (H_2 or ~2.7% H_2/Ar saturated with ~30 vol.% H_2O) at the other. The high moisture was maintained by bubbling fuel gas through a water bath kept at constant tempearture (~70 °C). All gas lines are wrapped with a heating tape kept at higher temperature (~100 °C) to minimize water condensation. A schematic drawing of the test set-up detailing the perimeter seal, the gas chamber and the electrical connections is given in Fig. 1 [23]. A hybrid mica seal with Ag interlayer was used as the perimeter seal for the chamber containing the reducing environment. The hybrid mica seal with Ag foil was recently reported to offer very long-term (>28,000 h) stability and thermal cycle stabil-

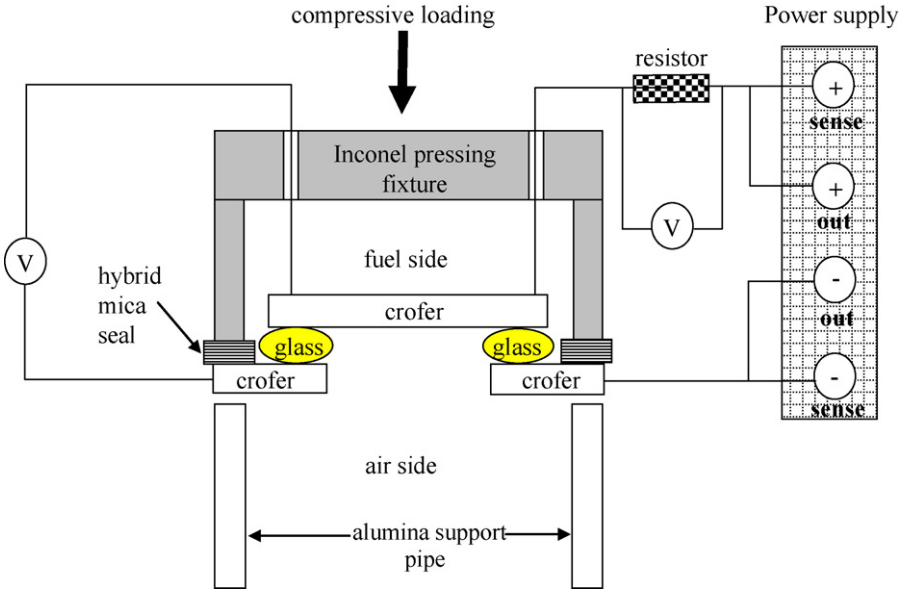

Fig. 1. Schematic drawing shows the set-up of the electrical stability test. The glass was sandwiched between two metal plates and sealed with compressive mica seals to provide a dual environment at elevated temperature. Platinum wires were used for measuring the voltage drop across a known resister and the sample (Ref. [19]).

Table 2
Thermal properties (in °C) of sealing glasses in the as-cast and crystallized state.

Glass/property	T_g	T_s	CTE × 10^{-6}
As-cast	645	693	11.76
Crystallized	N/A	916	11.68

ity over 1000 thermal cycles [24]. Four Pt-wires were spot-welded onto the sealed couples, two on the central square and two on the larger square but on the opposite side. A DC load of 0.7 V was applied with a commercial power supply (Agilent E3632A, Santa Clara, CA) on the sample. A known resistor was also connected in series to measure the current through the voltage drop with a multimeter (Aligent 34970A, Santa Clara, CA). The electrical stability tests were conducted in an accelerated manner at 850 °C or at the normal condition of 800 °C. After the test, the samples were characterized with optical microscopy. Some of the samples were also epoxy mounted, sectioned and polished for interfacial characterization using scanning electron microscopy (SEM) and energy dispersive spectroscopy (EDS) (JOEL SEM model 5900LV).

3. Results

3.1. Glass properties and spinel coating microstructure

Glass (YSO46) was modified from our earlier "refractory" sealing glass (YSO-1) [7] which has a composition in mole% of SrO(42.5%)–CaO(10%)–Y_2O_3(6%)–B_2O_3(7.5%)–SiO_2(34%). YSO-1 glass was readily crystallized and thermally stable with minimum change in CTE after long-term (1000-2000 h) aging in air or reducing environment but required higher sealing temperatures (~1000 °C). This high sealing temperature may promote undesirable and rapid oxidation when using ferritic stainless steels as candidate metallic interconnect materials. To lower the sealing temperatures we modified the glass composition by adding a small amount of ZnO (2.5%) and increased the B_2O_3 content from 7.5 to 10% (Table 1). B_2O_3 was found to be effective in lowering the glass forming temperatures due to its low melting point (~450 °C) and glass former nature as observed in many silicate glass systems and in our study [7]. However, the volatility of B_2O_3 at elevated temperatures may be an issue for long-term SOFC applications. Zheng et al. recently investigated the volatility of two Sr–Ca–Zn–B–Al–Ti–Si glasses (glass #59 and glass #27) [25]. They found that the volatile species with highest vapor pressure was BO_2(g) in dry air and $B_3H_3O_6$(g) in wet reducing gas for these sealing glasses. The cumulative weight loss for the glass (#59) containing 20% B_2O_3 was about 10× greater than glass (#27) containg 2% B_2O_3. However none of these glasses were tested with an active cell in SOFC environment and the effect of these volatile species remains to be determined.

Glass YSO46 was transparent and clear after casting from 1450 °C. The glass was then annealed at 600 °C for 6 h in air to relieve thermal stresses for better machining. The glass also remained clear and transparent on the surface and in the bulk after annealing, suggesting no crystallization in the current formulations. Thermal properties of glass transition point, softening point and average coefficient of thermal expansion (CTE) of the as-cast bulk glass and the sintered glass YSO46 (in powder compact form) are listed in Table 2. The linear thermal expansion behaviors are also shown in Fig. 2. The as-cast bulk glass showed typical expansion behavior of glasses with a distinct glass transition point where the slope rapidly increased (~645 °C), and a softening point (~693 °C). As compared to the parent glass (YSO-1), which had a transition point of 695 °C and softening point of 733 °C, the small increase of B_2O_3 (from 7.5% of glass YSO-1 to 10% of YSO46) was effective in lowering the thermal characteristics of the glass. The effect of a small addition of ZnO (2.5%) was not clear and the limited data would not be able to differentiate the effect of ZnO from B_2O_3. For the sintered glass, the linear thermal expansion showed different behavior without the distinct glass transition point, indicating rapid crystallization, consistent with the parent glass YSO-1 [7]. Fig. 3 shows the microstructure of the $Mn_{1.5}Co_{1.5}O_4$ spinel coating on Crofer22APU. The microstructure was not fully dense with scattered pores through the spinel layer of 5–6 μm thick. Underneath the spinel layer was a dense Cr-oxide scale of 2–3 μm thickness.

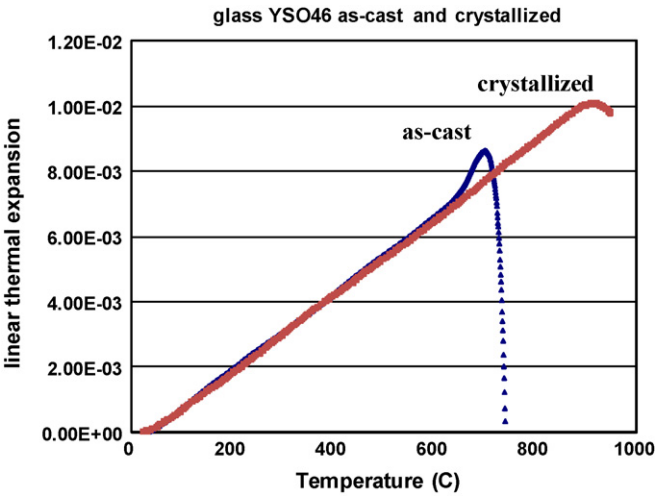

Fig. 2. Linear thermal expansion curves of glass YSO46 in the as-cast/annealed and short-term crystallized (950 °C/2 h, 800 °C/4 h) state.

3.2. Electrical stability in high moisture content fuel

The electrical stability tests of glass YSO46 with as-received and $(Mn,Co)_3O_4$ spinel coated Crofer22APU are shown in Figs. 4 and 5 for test temperature of 850 and 800 °C, respectively. The targeted operating temperature for the sealing glass is ~800 °C. The higher temperature of 850 °C was chosen to accelerate any interfacial reactions and/or diffusion across the glass/metal interface. The glass was exposed to ambient air at one side and flowing reducing gas at the other. The reducing condition in this dual environment was provided with dilute hydrogen (~2.7% H_2/Ar) saturated with ~30% H_2O. A high moisture fuel was chosen instead of dry hydrogen to more closely simulate operating conditions of real cells, in which medium to high fuel utilization is expected. The equilibrium PO_2 for this dilute moist hydrogen was calculated to be

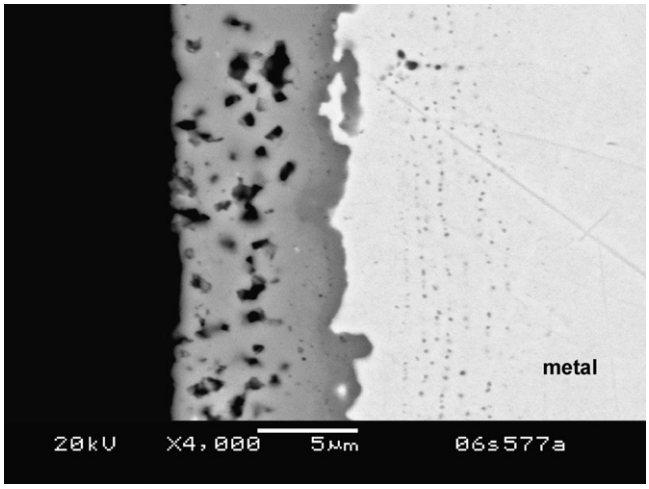

Fig. 3. Microstructure of the (Mn,Co)-spinel coated Crofer22APU.

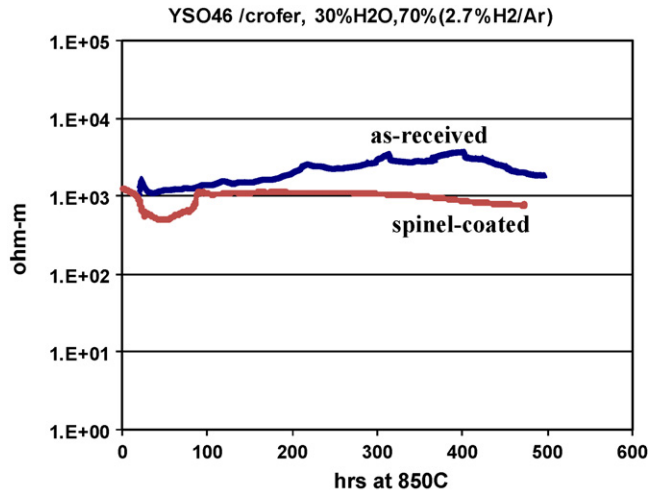

Fig. 4. Electrical stability test of glass YSO46 at 850 °C with Crofer22APU in the as-received and (Mn,Co)-spinel coated state in dual environment with dilute hydrogen (2.7% H_2/Ar) of high moisture content (30%).

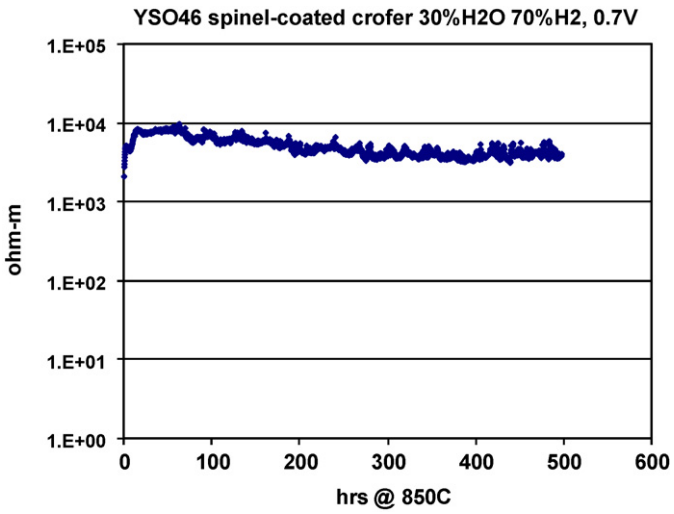

Fig. 6. Electrical stability test of glass YSO46 at 850 °C with Crofer22APU in the as-received and (Mn,Co)-spinel coated state in dual environment with pure hydrogen of high moisture content (30%).

1.0×10^{-16} atm. For comparison, the equilibrium PO_2 would be 9.5×10^{-19} atm for a pure hydrogen fuel saturated with the same amount of moisture. The initial resistivity at 850 °C of the glass sealed to either the as-received Crofer22APU or the (Mn,Co)-spinel coated Crofer22APU was similar, about ~10^3 Ω m (Fig. 4). The resistivity of the as-received sample showed gradual increase during isothermal ageing, reaching ~3.7×10^3 Ω m at ~400 h, and then decreased slightly to ~2×10^3 Ω m at ~500 h, while the resistivity of the (Mn,Co)-spinel coated sample appeared fairly constant at ~10^3 Ω m after the first ~100 h. For samples tested at 800 °C, the measured glass resistivities also showed similar values at the beginning of isothermal ageing: ~1.3×10^4 Ω m for the as-received sample and ~1.4×10^4 Ω m for the spinel coated one. The 800 °C resistivity appear to be an order of magnitude higher than 850 °C, typical of refractory ceramics and non-conducting glasses. The resistivity showed gradual increase with time for the as-received sample, reaching ~7.3×10^4 Ω m at ~460 h, while the spinel coated sample remained fairly constant at ~$1.0–1.4 \times 10^4$ Ω m for ~1000 h (Fig. 5). Overall, the measured resistivities appeared to be of the same magnitude as values previously reported in the literature.

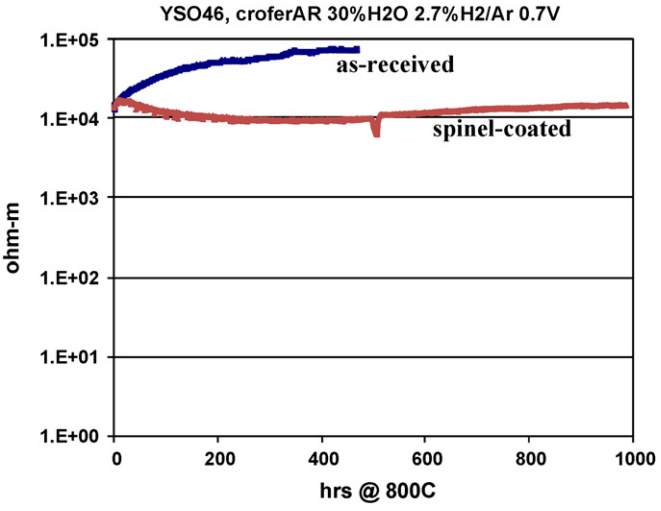

Fig. 5. Electrical stability test of glass YSO46 at 800 °C with Crofer22APU in the as-received and (Mn,Co)-spinel coated state in dual environment with dilute hydrogen (2.7% H_2/Ar) of high moisture content (30%).

For example, Haanappel et al. reported an electrical resistivity for a Ba(41.4%)–Ca(8.6%)–Si(34.7%) glass containing small additives of Al, B, Zn, V and Pb of ~$2–10 \times 10^4$ Ω m at 800 °C with a similar ferritic stainless steel of low Si (<0.01) and Al (<0.01) contents [22]. Chou et al. reported a resistivity of ~3.2×10^4 Ω m for a similar alkaline-earth silicate glass on as-received Crofer22APU at 800 °C after aging for 500 h in similar dual environment [26].

In addition to the tests in dilute hydrogen (2.7%H_2/Ar), we also tested the glass in a more reducing environment by using pure hydrogen and the same amount of moisture (30%). The electrical resistivity for the (Mn,Co)-spinel coated sample at 850 °C vs. time is shown in Fig. 6. Clearly the glass again demonstrated good electrical stability with a resistivity of ~4×10^3 Ω m after ~200 h aging, consistent with samples tested in dilute hydrogen.

3.3. Post-mortem microstructure and interface characterization

3.3.1. As-received Crofer22APU sample

Samples tested at 850 °C in dilute and moist hydrogen using the as-received and (Mn,Co)-spinel coated Crofer22APU were subjected to microstructure and interfacial analysis. Fig. 7 shows the microstructure at the glass/as-received Crofer22APU metal interface in two locations: the center of the glass seal (Fig. 7A) and the edge of the seal exposed to air (Fig. 7B). The locations of these two areas are shown in the inset drawing. Chemical analyses by energy dispersive spectroscopy of selected points in these two areas are listed in Tables 3 and 4 for the center and edge location, respectively. At the central location, where the glass was sealed between the two metal couples, it is evident that the glass sealed metal still formed a thick Cr-oxide layer (~3–7 μm) on top of the as-received Crofer22APU matrix (point #1 in Fig. 7A). Next to this gray region is a thin dark layer (point #2 in Fig. 7A) about 2 μm thick. The layer consists of Cr, Si, Mn, Sr, Zn and Fe (at.% in decending order). The observed Cr-oxide layer and layer containing (Cr,Mn) were consistent with earlier reports that these oxides tended to form on ferritic stainless steel whether in air or reducing environments [22,27]. Next to the dark thin layer were some angular crystals of 1–3 μm in size (point #3 in Fig. 7A). EDS of these crystals showed they contained primarily Sr, Ba and Cr with the atomic ratio of (Sr + Ba)/Cr ~1 (Table 3), indicating they were Sr or Ba chromates, which were previously found at interfaces of alkaline-earth silicate glass with Cr-containing ferritic stainless steels near the air side [13,14]. There were also some large grains next to the smaller chromate grains

Table 3
Chemical analysis of points #1–4 in Fig. 7A (in at.%).

#/element	O	Si	Ti	Cr	Mn	Fe	Zn	Sr	Ba
1	31.29	–	0.45	67.34	–	0.92	–	–	–
2	48.91	18.28	–	20.61	4.96	1	1.75	4.48	–
3	46.04	–	–	26.67	–	–	–	25.4	1.89
4	19.48	9.47	–	40.11	–	–	–	25.57	5.38

Table 4
Chemical analysis of points #1–3 in Fig. 7B (in at.%).

#/element	O	Si	Ca	Cr	Fe	Y	Sr	Ba
1	47.50	0.84	–	43.59	6.49	–	1.58	–
2	47.99	–	0.62	26.59	0.65	–	23.04	1.11
3	49.01	25.27	2.27	2.49	–	8.84	12.12	–

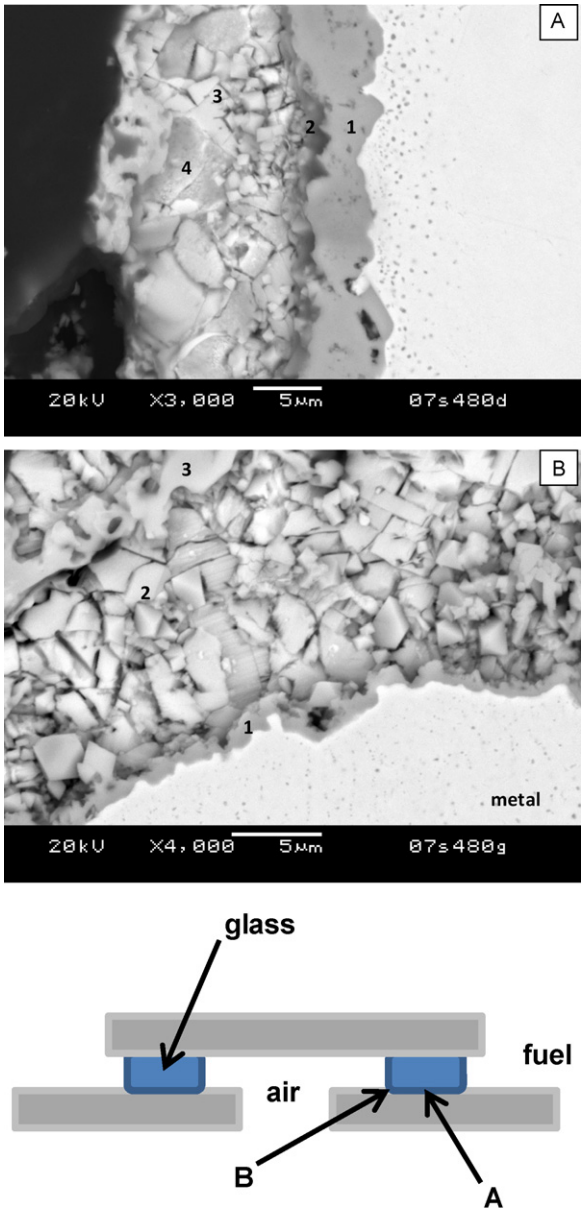

Fig. 7. SEM micrograph shows the interfacial microstructure of the as-received Crofer22APU/glass sample after electrical stability test at 850 °C for ~500 h in dual environment: (A) central location and (B) near air side. The location of (A) and (B) is shown in the inset.

(point #4 in Fig. 7A) containing not only Sr, Ba and Cr but also Si. The angular morphology of these large grains (instead of rounded shape) suggested they were not residual glassy phases. For alkaline-earth silicate glasses where the alkaline-earth (Sr or Ba) and Si were the main constituents the major crystalline phases after devitrification were identified as $SrSiO_3$ [7], $BaSiO_3$ and $BaAl_2Si_2O_8$ if the glass also contained Al_2O_3 [6]. No particular crystalline phase was found from the EDS analysis of point #4. As for the glass/metal interface near the air side edge, the angular chromate grains (#2 in Fig. 7B) were much more abundant while the Cr-oxide layer (#1 in Fig. 7B) appeared much thinner (Fig. 7B). The Cr-oxide layer was about <1 μm and the (Sr,Ba) chromate layer reached about 10 μm. Outside the chromate layer was the sealing glass (#3). The much thinner Cr-oxide layer and thicker chromate layer was not surprising that the formation of chromate at air side is thermodynamically favorable by either of the following reactions [7]:

$$2SrO + Cr_2O_3 + 3/2O_2 = 2SrCrO_4 \quad (1)$$

$$2SrSiO_3 + Cr_2O_3 + 3/2O_2 = 2SrCrO_4 + 2SiO_2 \quad (2)$$

In the presence of oxygen, the newly formed Cr-oxide layer can continuously react with Sr-oxides to form the chromate. As a result, no thick Cr-oxide layer was formed and the thick chromate layer observed instead. It is interesting to note that the thick chromate layer did not result in debonding along the interface since large residual stresses were expected along the interfaces and within the chromate grains because of the very high CTEs (~22–23 × 10^{-6}/°C) and anisotropy of Sr or Ba chromates [28].

3.3.2. (Mn,Co)-spinel coated Crofer22APU sample

The microstructure at the glass/metal interface of the (Mn,Co)-spinel coated sample after the 850 °C ~500 h electrical stability test is shown in Fig. 8. Two locations were selected for analysis: one at the center of the sealing glass (Fig. 8A) and one at the air side edge (Fig. 8B). The locations of these two spots are also shown in the inset of Fig. 7. Selective points at these two locations were also subjected to EDS analysis and the chemical compositions are listed in Tables 5 and 6 for the central and air side edge, respectively. In the central area, where the glass/metal interface was at an equal distance from the air side and the fuel side, the interfacial microstructure was very different from the as-received sample. Next to the metal substrate was a very thin (~1 μm) dense oxide layer (point #1 in Fig. 8A) consisting primarily of Cr (~48%) but also containing Mn (~3%) and Fe (~16%). In contrast, the Cr-oxide was much thicker for the as-received one (Fig. 7A). This is likely due to the protection from the (Mn,Co)-spinel coating which minimized the oxygen transport to the bare metal substrate. Next to this thin layer was another thin dense (~1 μm) layer (point #2) containing more Mn (~11%) and less Fe (~6%), but also Co (~6%) and some Zn and Sr. The initial chemical composition of the spinel coating

Table 5
Chemical analysis of points #1–6 in Fig. 8A (in at.%).

#/element	O	Si	Ca	Cr	Mn	Fe	Co	Zn	Sr	Y
1	33.09	0.44	–	47.97	2.91	15.59	–	–	–	–
2	37.84	0.56	–	35.86	11.12	4.53	5.55	2.76	1.66	–
3	41.85	0.89	–	27.04	12.18	5.65	5.61	2.30	3.74	0.74
4	38.21	25.03	1.01	–	6.58	–	3.99	1.95	23.22	–
5	46.76	12.8	5.19	–	0.79	–	–	–	19.8	14.66

Table 6
Chemical analysis of points #1–3 in Fig. 8B (in at.%).

#/element	O	Si	Ti	Cr	Mn	Fe	Co	Zn	Sr	Ba
1	43.87	0.81	–	30.47	8.42	6.07	4.05	4.9	1.41	–
2	48.07	–	0.73	28.96	–	1.31	–	–	20.92	–
3	40.37	0.85	–	33.03	9.15	6.33	4.37	5.27	0.63	–
4	49.57	–	–	24.52	–	–	–	–	21.99	3.93

was $Mn_{1.5}Co_{1.5}O_4$ (equal mole ratio of Mn–Co). The excess of Mn (instead of Mn:Co = 1:1) in points #2 and 3 was likely from the metal substrate that Mn is known to diffuse outward faster than Cr and often forms a thin (Cr,Mn) oxide layer or particles on top of the Cr-oxide layer for these ferritic stainless steels [13]. Above these layers was a porous region with some large grains (point #3) which had a similar composition to point #2. Above this porous region was a rather dense thick layer without distinct features (point #4) which primarily showed the alkaline silicate glass with some Mn (~6.6%) and Co (~4%), indicating some dissolution of the spinel coating into the glass. Away from this ~10 μm dense layer was the sealing glass with only a trace amount of Mn (~0.8%). It is interesting to note that within the spinel region (#2 and 3) elements from the sealing glass showed very different proportions from the parent glass, particularly Zn and Sr, respectively. The presence of Sr was likely due to the thermodynamically favorable chromate formation while the presence of Zn was not clearly understood. Zn in alkaline-earth silicate sealing glass was found to form $Ca_2ZnSi_2O_7$ when aged 1 week at 800 °C [29]. The reaction of Zn with (Mn,Co)-spinel is unknown and may not be an issue with a glass of low Zn content.

The glass/metal interface near the air side edge was also examined (Fig. 8B). Point #1 showed the typical Cr-oxide layer, about ~2 μm thick, but also contained appreciable amounts of Mn, Fe, Co and Zn. Next to the Cr-oxide was a layer (about 5 μm thick) of discrete grains (point #2) with primarily Sr and Cr and trace of Fe and Ti, likely $SrCrO_4$. Point #3 also contained a substantial amount of Cr (~33%) and Mn, Fe, Co and Zn from ~9 to ~4%, with a trace of glass constituents such as Si and Sr, respectively. The next region consisted primarily of chromates with (Sr + Ba)/Cr ~1. From the original spinel coating microstructure and both Figs. 7 and 8 after the ~500 h ageing, it is evident that the current sealing glass reacted severely with the (Mn,Co)-spinel layer, with no distinct (Mn,Co)-spinel layer remaining after the test.

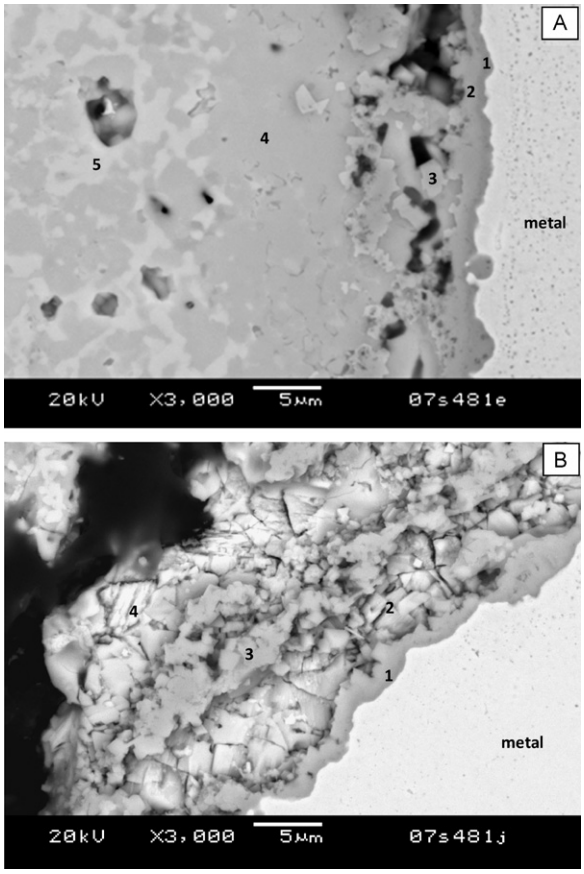

Fig. 8. SEM micrograph shows the interfacial microstructure of the (Mn,Co)-spinel coated Crofer22APU/glass sample after electrical stability test at 850 °C for ~500 h in dual environment: (A) central location and (B) near air side. The location of (A) and (B) is shown in the inset of Fig. 7.

4. Discussion

4.1. Electrical stability of sealing glass

The measured electrical resistivity of the Sr–Ca–Y–B–Si–Zn glass was in the range of $\sim 10^3$ to $10^5\ \Omega$ m in the temperature range of 800–850 °C. Such high resistivity can be considered insulating as compared to active SOFC cell materials. For example, the electrical resistivity of YSZ electrolyte at 800 °C is $\sim 2.5 \times 10^{-1}\ \Omega$ m, $6.7 \times 10^{-5}\ \Omega$ m for typical LSM cathode and contact and $3.3 \times 10^{-5}\ \Omega$ m for Ni/YSZ anode support. The resistivities of Ni contact and metallic interconnect such as Crofer22APU would be even lower. As a result, the electrical loss through the sealing glasses would be negligible. In our electrical ageing test under DC load, the limited data from ~500 to ~1000 h showed reasonable stability without a rapid decrease with time. For stationary applications, all SOFC materials including cells, interconnect, contact and seals should be able to last ~40,000 h without substantial degradation, whether it is chemical, thermal, electrical or mechanical. The challenge of glass sealing is that most of the changes/degradation are not independent of each other. For example, a change in thermal properties as CTE over ageing could also have a direct impact on mechanical integrity of the seal. Likewise, severe reaction at the glass/metal interface such as chromate formation could very well degrade the seal strength substantially [14,15]. In this study,

the Sr–Ca–Y–B–Si–Zn sealing glass was modified from a previous "refractory" sealing glass of very similar chemical compostions. The composition of these glass often has less numbers of bridging oxygen per SiO_4 tetrahedron could lead to rapid crystallization as is our system and the glass turned into a glass–ceramics after initial sealing. The crystallized glass would thus be thermally more stable if the crystalline phases remained unchanged over ageing. Our previous study of the parent glass showed very stable microstructure and thermal properties over ~2000 h ageing [7]. The electrical conductivity of typical ceramics–glass depends on the charge of conducting ion, its mobility and concentration. From a mobility point of view, a free ion in a glassy phase would be much more mobile than ions "locked" into a crystalline structure or required to move between crystallites. Therefore the long-term electrical stability of the current glass would be not be a concern for SOFC applications.

4.2. (Mn,Co)-spinel coating for sealing area

The $Mn_{1.5}Co_{1.5}O_4$ spinel coating was originally developed for cathode protection from Cr-poisoning due to its ability to prevent Cr volatility from steel interconnects, high conductivity, good CTE match to ferritic stainless steels and good stability at elevated temperature in air [19]. The current evaluation of an alkaline-earth sealing glass in terms of electrical stability proved the spinel coating to be a viable coating for sealing areas, at least from an electrical insulation point of view, as compared to a separate coating such as aluminization for sealing areas alone. Nevertheless, substantial degradation of the coating structure by the sealing glass was evident in that the relative dense spinel layer (Fig. 3) was broken down to discrete particles or islands as shown in Fig. 8A and B after ~500 h ageing at 850 °C. It is likely the molten sealing glass during firing (at 950 °C) corroded or dissolved the spinel structure; however, no particular crystalline phases containing Mn or Co were identified within the corroded/dissolved spinel region. The undesirable chromates were still formed at the air side; however, not in the sealing central section. This behavior differed from the as-received sample where chromates were also formed in the central section (Fig. 7A). The chemical stability of $Mn_{1.5}Co_{1.5}O_4$ spinel coating on AISI 430 has been investigated by Yang et al. in a reducing environment (2.75% H_2/bal. Ar with ~3% H_2O) [19]. They found that the spinel decomposed to MnO and Co metal after 24 h exposure at 800 °C. In our spinel coated sample, no spinel decomposition occurred since no individual MnO and Co metal particles were present at the glass/metal interface at the central sealing section, indicating the the local PO_2 was not reducing enough to decompose the structure. However, one may expect to see the decomposition of spinel at the fuel side edge. Overall, the observed chromate formation at the air side and the instability of the spinel phase in reducing atmospheres and when in contact with the glass seal suggests that the spinel coatings are not viable as protective coatings for glass seal/steel interconnect interfaces.

5. Conclusion

A novel alkaline-earth yttrium silicate sealing glass (Sr–Ca–Y–B–Si–Zn) was developed and used to test the electrical stability with and without (Mn,Co)-spinel coating on Crofer22APU. All samples, whether with as-received or spinel coated Crofer22APU, showed desirable electrical stability with resistivity in the range of $\sim 10^3$–$10^5\ \Omega$ m at 800–850 °C for 500–1000 h under a DC load of 0.7 V under dual atmosphere exposure conditions. After testing, the microstructure at the glass/metal interfaces was characterized. For as-received samples, chromates were found at both air side and central locations. For the spinel coated samples, chromate was found only at the air side edges. The spinel layer was apparently attacked by the sealing glass such that the continuous spinel layer was broken into particles and islands. Although the electrical resistivity showed good stability, the observed structural degradation indicated that the (Mn,Co)-spinel coating is not suitable for SOFC interconnect sealing areas.

Acknowledgements

The authors would like to thank S. Carlson for SEM sample preparation and J. Coleman for SEM analysis. This work summarized in this paper was funded by the US Department of Energy's Solid-State Energy Conversion Alliance (SECA) Core Technology Program. The authors would like to thank Wayne Surdoval and Briggs White from NETL for helpful discussions. Pacific Northwest National Laboratory is operated by Battelle Memorial Institute for the US Department of Energy under Contract no. DE-AC06-76RLO 1830.

References

[1] N.Q. Minh, Ceramic fuel cells, J. Am. Ceram. Soc. 76 (3) (1993) 563–588.
[2] B.C.H. Steele, Materials science and engineering: the enabling technology for the commercialization of fuel cell systems, J. Mater. Sci. 36 (2001) 1053–1068.
[3] S.C. Singhal, "Progress in tubalar solid oxide fuel cell technology," in Solid Oxide Fuel Cells (SOFC VI), in: Proceedings of the Sixth International Symposium, Edited by S.C. Singhal and M. Dokiya, Proceedings Volume 99–19, The Electrochemical Society, 1999, pp. 39–51.
[4] R. Bolden, K. Foger, T. Pham, "Towards the development of a 25 kW planar SOFC system," in Solid Oxide Fuel Cells (SOFC VI), in: Proceedings of the Sixth International Symposium, Edited by S.C. Singhal and M. Dokiya, Proceedings Volume 99–19, The Electrochemical Society, 1999, pp. 80–87.
[5] A. Khandkar, S. Elangovan, J. Hartvigsen, D. Rowley, R. Privette, M. Tharp, "Status and progress in SOFCo's planar SOFC development," in Solid Oxide Fuel Cells (SOFC VI), in: Proceedings of the Sixth International Symposium, Edited by S.C. Singhal and M. Dokiya, Proceedings Volume 99–19, The Electrochemical Society, 1999, pp. 88–94.
[6] K.D. Meinhardt, D.-S. Kim, Y.-S. Chou, K.S. Weil, Synthesis and properties of a barium aluminosilicate solid oxide fuel cell glass–ceramic sealant, J. Power Sources 182 (1) (2008) 188–196.
[7] Y.-S. Chou, J.W. Stevenson, P. Singh, Novel refractory alkaline earth silicate sealing glasses for planar solid oxide fuel cells, J. Electrochem. Soc. 154 (7) (2007) B644–B651.
[8] N. Lahl, K. Singh, L. Singheiser, K. Hilpert, D. Bahadur, Crystallization kinetics in $AO–Al_2O_3–SiO_2–B_2O_3$ glasses (A = Ba, Ca, Mg), J. Mater. Sci. 35 (2000) 3089–3096.
[9] S.-B. Sohn, S.-Y. Choi, G.-H. Kim, H.-S. Song, G.-D. Kim, Stable sealing glass for planar solid oxide fuel cell, J. Non-cryst. Solids 297 (2002) 103–112.
[10] K.L. Ley, M. Krumpelt, R. Kumar, J.H. Meiser, I. Bloom, Glass–ceramic sealants for solid oxide fuel cells. Part I. Physical properties, J. Mater. Res. 11 (6) (1996) 1489–1493.
[11] X. Qi, F.T. Akin, Y.S. Lin, Ceramic–glass composite high temperature seals for dense ionic-conducting ceramic membranes, J. Membr. Sci. 193 (2001) 185–193.
[12] N. Lahl, D. Bahadur, K. Singh, L. Singheiser, K. Hilpert, Chemical interactions between aluminosilicate base sealants and the components on the anode side of solid oxide fuel cells, J. Electrochem. Soc. 149 (5) (2002) A607–A614.
[13] Z. Yang, K.D. Meinhardt, J.W. Stevenson, Chemical interactions of barium–calcium–aluminosilicate-based sealing glass with ferritic stainless steel interconnect in SOFCs, J. Electrochem. Soc. 150 (8) (2003) A1095–A1101.
[14] Y.-S. Chou, J.W. Stevenson, P. Singh, Effect of pre-oxidation and environmental aging on the seal strength of a novel high-temperature solid oxide fuel cell (SOFC) sealing glass with metallic interconnect, J. Power Sources 184 (1) (2008) 238–244.
[15] Y.-S. Chou, J.W. Stevenson, P. Singh, Effect of aluminizing of Cr-containing ferritic alloys on the seal strength of a novel high-temperature solid oxide fuel cell sealing glass, J. Power Sources 184 (2) (2008) 1001–1008.
[16] H. Yokokawa, T. Horita, N. Sakai, K. Yamaji, M.E. Brito, Y.-P. Xiong, H. Kishimoto, Thermodynamic considerations on Cr poisoning in SOFC cathodes, Solid State Ionics 177 (2006) 3193–3198.
[17] S. Taniguchi, M. Kadowaki, H. Kawamura, T. Yasuo, Y. Akiyama, Y. Miyake, T. Saitoh, Degradation phenomena in the cathode of a solid oxide fuel cell with an alloy separator, J. Power Sources 55 (1) (1995) 73–79.
[18] S.P. Simner, M.D. Anderson, G.G. Xia, Z.G. Yang, L.R. Pederson, J.W. Stevenson, SOFC performance with Fe–Cr–Mn alloy interconnect, J. Electrochem. Soc. 152 (4) (2005) A740–A745.

[19] Z. Yang, G. Xia, X. Li, J.W. Stevenson, $(Mn,Co)_3O_4$ spinel coatings on ferritic stainless steels for SOFC interconnect applications, Int. J. Hydrogen Energy 32 (16) (2007) 3648–3654.
[20] J. Wu, Y. Jiang, C. Johnson, X. Liu, DC electrodeposition of Mn–Co alloys on stainless steels for SOFC interconnect application, J. Power Sources 177 (2) (2008) 376–385.
[21] W. Wei, W. Chen, D.G. Ivey, Oxidation resistance and electrical properties of anodically electrodeposited Mn–Co oxide coatings for solid oxide fuel cell interconnect applications, J. Power Sources 186 (2) (2009) 428–434.
[22] V.A.C. Haanappel, V. Shemet, S.M. Gross, Th. Koppitz, N.H. Menzler, M. Zahid, W.J. Quadakkers, Behavior of various glass–ceramics sealants with ferritic steels under simulated SOFC stack conditions, J. Power Sources 150 (2) (2005) 86–100.
[23] Y.S. Chou, J.W. Stevenson, K.D. Meinhardt, Electrical stability of a novel refractory sealing glass in dual environment for solid oxide fuel cell applications, J. Am. Ceram. Soc. 93 (3) (2010) 618–623.
[24] Y.-S. Chou, J.W. Stevenson, Long-term ageing and materials degradation of hybrid mica compressive seals for solid oxide fuel cells, J. Power Sources 191 (2) (2009) 384–389.
[25] T. Zheng, R.K. Brow, S.T. Reis, C.S. Ray, Borate volatility from SOFC sealing glasses, J. Am. Ceram. Soc. 91 (8) (2008) 2564–2569.
[26] Y.-S. Chou, J.W. Stevenson, K.D. Meinhardt, Electrical stability of a novel refractory sealing glass in dual environment for solid oxide fuel cell applications, J. Am. Ceram. Soc. (2009).
[27] E. Konysheva, U. Seeling, A. Besmehn, L. Singheiser, K. Hilpert, Chromium vaporization of the ferritic steel Crofer22APU and ODS Cr5Fe1Y2O3 alloy, J. Mater. Sci. 42 (14) (2007) 5778–5784.
[28] C.W.F.T. Pistorius, M.C. Pistorius, Z. Kristallogr. 117 (1962) 259.
[29] T. Zhang, R.K. Brow, S.T. Reis, C.S. Ray, Isothermal crystallization of a solid oxide fuel cell sealing glass by differential thermal analysis, J. Am. Ceram. Soc. 91 (10) (2008) 3235–3239.